Magnetic Resonance Imaging 62 (2019) 111–120

Contents lists available at ScienceDirect

Magnetic Resonance Imaging

journal homepage: www.elsevier.com/locate/mri

Original contribution

Quantification of breast tissue density: Correlation between single-sided portable NMR and micro-CT measurements

Xuan Huang[a,b,c], Tonima S. Ali[a,d], Teresa Nano[e], Tony Blick[a,b], Brian Wan-Chi Tse[f], Kamil Sokolowski[f], Monique C. Tourell[a,d], Thomas Lloyd[g], Erik W. Thompson[a,b,c,h], Konstantin I. Momot[a,d,1], Honor J. Hugo[a,b,c,*,1]

[a] Institute of Health and Biomedical Innovation, Queensland University of Technology (QUT), Brisbane, Australia
[b] Translational Research Institute, Woolloongabba, Australia
[c] School of Biomedical Sciences, Faculty of Health, Queensland University of Technology (QUT), Brisbane, Australia
[d] School of Chemistry, Physics and Mechanical Engineering, Queensland University of Technology (QUT), Brisbane, Australia
[e] Greenslopes Private Hospital, Greenslopes, Australia
[f] Preclincal Imaging Facility, Translational Research Institute, Woolloongabba, Australia
[g] Radiology Department, Princess Alexandra Hospital, Woolloongabba, Australia
[h] University of Melbourne, Department of Surgery, St. Vincent's Hospital, Melbourne, Australia

ARTICLE INFO

Keywords:
Breast imaging
Mammographic density
Single-sided portable NMR
μCT
Diffusion
Spin-relaxation rate constants T_1 and T_2

ABSTRACT

Mammographic density (MD) is a strong independent risk factor for breast cancer. Traditional screening for MD using X-ray mammography involves ionising radiation, which is not suitable for young women, those with previous radiation exposure, or those having undergone a partial mastectomy. Therefore, alternative approaches for MD screening that do not involve ionising radiation will be important as the clinical use of MD increases, and as more frequent MD testing becomes desirable for research purposes. We have previously demonstrated the potential utility of spin relaxation-based, single-sided portable-NMR measurements for the purpose of MD quantification. We present here a more refined analysis by quantifying breast tissue density in excised samples on a continuous scale (0% to 100% fibroglandular tissue content) using micro-CT (μCT), and comparing the results to spin-relaxation and diffusion portable-NMR measurements of the same samples. μCT analysis of mammary tissues containing high- and low-MD (HMD and LMD, respectively) regions had Hounsfield Unit (HU) histograms with a bimodal pattern, with HMD regions exhibiting significantly higher HU values than LMD regions. Quantitative MD (%HMD) values obtained using μCT exhibited an excellent correlation with portable-NMR results, namely longitudinal spin-relaxation time constants (T_1) and the relative tissue water content obtained from portable-NMR diffusion measurements ($R^2 = 0.92$, $p < 0.0001$ and $R^2 = 0.96$, $p < 0.0001$, respectively). These findings are consistent with our previous results demonstrating relatively high water content in HMD breast tissue, consistent with the high proportion of fibroglandular tissue, FGT, which in turn contains more abundant water-carrying HSPG proteins. We observed an excellent correlation between the T_1 values and diffusion NMR-measured relative tissue water content ($R^2 = 0.94$, $p < 0.0001$). These findings demonstrate, for the first time, the ability of single-sided portable NMR to accurately quantify MD *in vitro* on a continuous scale. The results also indicate that portable-NMR analysis can assist in the identification of features underpinning MD, namely FGT and adipose tissue content. Future work will involve application of portable NMR to quantifying MD *in vivo*.

1. Introduction

Mammographic density (MD), also known as breast density, reflects the relative amounts of fibroglandular tissue (FGT) and adipose tissue ("fat") in the breast. MD is highly clinically significant due to its relationship to both the risk of developing breast cancer and the reliability of imaging-based detection of breast cancer, which is discussed below. MD is traditionally quantified using X-ray mammography, the

* Corresponding author at: Institute of Health and Biomedical Innovation, Queensland University of Technology (QUT), Brisbane, Australia.
E-mail address: honor.hugo@qut.edu.au (H.J. Hugo).
[1] Denotes equal senior authors.

https://doi.org/10.1016/j.mri.2019.06.006
Received 4 February 2019; Received in revised form 23 May 2019; Accepted 6 June 2019

breast cancer screening method recommended by the World Health Organization [1] and provided to women aged 40–74 by BreastScreen in Australia [2]. In mammograms, high-MD regions, representing epithelial and stromal tissue, have a high-intensity (bright) radiographic appearance. Conversely, non-dense (fatty) breast tissue has a low-intensity (dark) appearance on a mammogram. The extent of density of the breast is commonly represented by a Breast Imaging Reporting and Data System (BI-RADS) score. The efficacy of mammography for cancer detection is significantly lowered when the breast is extremely dense mammographically (> 75% dense tissue, BI-RADS category d [3]), 62.2% in comparison to 88.2% in a fatty breast (BI-RADS category a) [4]. High MD score is also an independent breast cancer risk factor after adjustment for age and body mass index [5]. Approximately 8% of all women aged 40–74 have extremely dense breasts [6]. For these women the risk of developing breast cancer in their lifetime is approximately 4–5 times higher than for those with a low MD score, and approximately 2-fold higher than for the general population [7]. It may ultimately be valuable to accurately quantify the breast density of women and hence obtain a more accurate assessment of their breast cancer risk. Furthermore, change in MD on the time scale of weeks or months has potential as a predictive marker of response of women to antiestrogens used in both chemoprevention in the high risk setting, or as an adjuvant therapy for oestrogen receptor-positive breast cancers [8,9]. Recent studies have indicated that the potential use of assessing change in MD as a predictive biomarker may also extend to other breast cancer therapies [10]. Therefore, high-frequency observation of MD may find utility in monitoring treatment response. However, monitoring this change through repeated mammography, which involves repeated exposure to X-rays, is not clinically justifiable due to the high added cancer risk. Mammography is also clinically unsuitable for young women, those with previous significant radiation exposure, or those having undergone a partial mastectomy.

Potential approaches to MD assessment that are free of ionising radiation include automated breast ultrasound, ultrasound elastography and transillumination breast spectroscopy, which display reasonable concordance with mammography, and magnetic resonance imaging (MRI). Fibroglandular tissue (FGT) content derived from T_1-weighted clinical MRI exhibits one of the best observed correlations with MD [11]. However, clinical MRI is relatively costly and requires infrastructure typically only available in major hospitals, which limits its utility for women who live in rural and remote areas.

Portable NMR has remarkable translational potential in that it offers much of the flexibility and sensitivity of clinical MRI without the high cost (both per scanning unit and per individual scan). It is compact and portable, which means that it can be easily deployed outside of a specialist facility. Crucially, like clinical MRI, portable NMR does not employ ionising radiation or uncomfortable breast compression inherent in mammography. Furthermore, portable NMR is free of claustrophobia-related patient discomfort that can be associated with clinical MRI.

We have previously shown that a commercially available portable-NMR instrument, NMR-Mouse, enables discrimination between regions of high and low MD (HMD and LMD, respectively) *via* longitudinal spin-relaxation rate constants, T_1, [12,13] and the relative amplitudes of fat and water peaks in T_2 spectra [12,13]. However, there are notable limitations to those studies (summarised in Table 1), the most important of which is the binary nature of the HMD/LMD classification: the mammographic images used in those studies as a MD "gold standard" were used only to identify "HMD regions" and "LMD regions" within the samples and were not used to assess breast density as a continuous entity. The other significant limitation was that the model of the instrumentation used, NMR-Mouse PM5, enabled measurements only up to a 5 mm penetration depth. While this limitation was immaterial in the measurements of excised samples *in vitro*, it could potentially limit the utility of portable-NMR measurements *in vivo*.

We address these limitations in the present study by quantifying MD on a continuous scale, as opposed to the binary HMD/LMD categorisation. We used a mammogram image of the breast slice to guide selection of smaller breast tissue specimens across a wide range of mammographic densities, and then imaged these smaller excised samples using μCT. This enabled detailed volumetric 3D reconstruction of the MD distribution within the samples. Volume-averaged mammographic density of each sample was quantified based on the relative areas of the water and fat peaks in the histograms of the Hounsfield Unit values derived from the 3D maps. We then subjected the same samples to a range of portable-NMR measurements (T_1, T_2 and diffusion) and examined the correlation between portable-NMR and μCT results with a view of assessing the utility of portable NMR as a tool for continuous-scale quantification of MD.

2. Methods

2.1. Details of the two patients and breast tissue explants used in this study

Two human breast tissue specimens with no evidence of malignancy were accrued each from high-risk prophylactic mastectomy surgeries at the Greenslopes Private Hospital, Brisbane. The study was approved by the Metro South Hospital and Health Services, Queensland (HREC/16/QPAH/107), and conducted in accordance with the Australian National Statement on Ethical Conduct in Human Research (2007). Women were excluded from this study if they had suspicious ductal carcinoma *in situ* or microcalcifications on radiological investigations. BI-RADS density scores were estimated from the pre-surgery mammogram. Post-surgery, mammography was performed on 1–1.5 cm thick un-fixed, craniocaudal slices of mammary tissue surplus to pathologists' needs, and areas of high, medium and low MD were denoted by a radiologist. Ten samples of breast tissue, approximately $(7\ \text{mm})^3$ in size, from a range of mammographically dense regions were then excised for analysis. Two different women were involved in this study; patient 1 was of BiRADs density category 3 (a) and patient 2 of BiRADs 4 (d) and both were premenopausal. However the purpose of this study was not to compare %HMD or NMR T1 values to this information, but to each other.

2.2. μCT and MD measurements

Excised pieces of breast tissue were placed inside a cylindrical 50 mL Corning™ Falcon™ tube (Corning, Mulgrave, Victoria), with moist tissue paper placed at the end distal to the specimen in order to limit dehydration. The tube was then placed horizontally inside an Inveon μCT scanner (Siemens Medical Solutions), and μCT images were

Table 1
How the approaches taken in the current study differ from our previous work.

	References [12, 13]	Current study
Sample density range	Binary; 5 pairs of HMD *vs* LMD samples	Continuous; 10 samples representing a range of densities
Maximum penetration depth	5 mm (NMR-Mouse PM5)	25 mm (NMR-Mouse PM25)
NMR-measured quantities	T_1 [12] and the relative area of the water T_2 peak [13].	T_1, T_2 and relative water content from diffusion measurements
Gold-standard MD measurements	2D (mammography)	3D (μCT)
Statistical measure	Statistically significant difference between HMD and LMD regions	Unilateral linear regression
MD outputs	"High" *versus* "Low"	Plot of density distribution throughout sample, % HMD

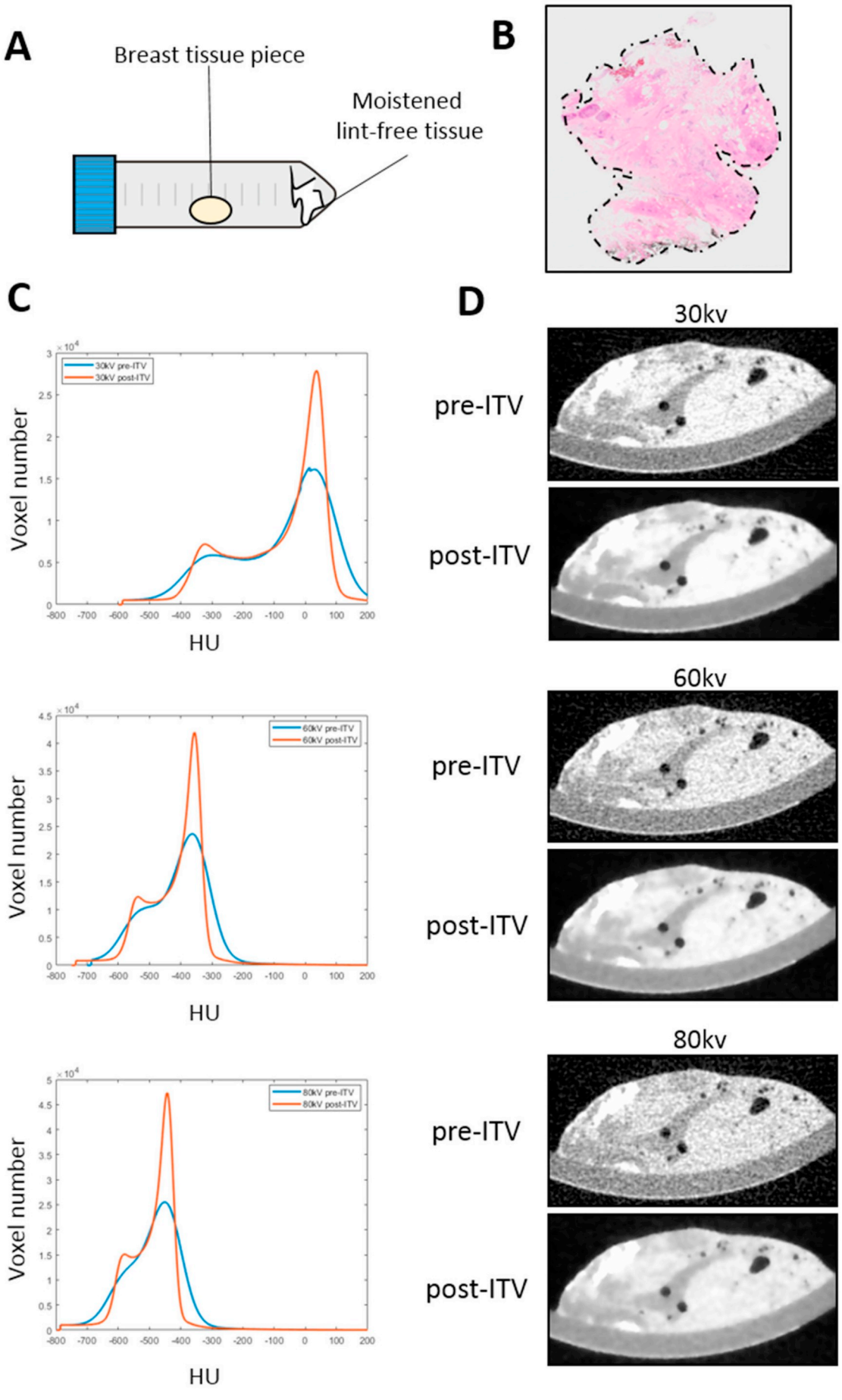

(caption on next page)

Fig. 1. Optimization of the microCT (μCT) protocol for breast tissue slices. A. All tissue slices were scanned within a round-walled tube to minimize machine noise due to scanning artefacts generated from sharp-walled vessels. B. Haematoxylin and Eosin stain of formalin-fixed, paraffin-embedded mammary tissue used in optimization, depicting a range of density (high dense: intense pink corresponding to stroma and glandular tissue, low dense; fat is washed out in processing of tissue for paraffin embedding so appears white). C. Density distribution plots before and after ITV de-noising, voxel number distribution is presented according to HU (Hounsefield Units). D. Comparable 2D view through the 3D x-ray of the tissue before and after the ITV de-noising protocol was applied. Exposure time for the 60 kV protocol was 530 ms, and for 80 kV was 300 ms. For both, projection numbers were 180, 0.5uA current, binning factor of 2, and medium-low magnification. (For interpretation of the references to colour in this figure legend, the reader is referred to the web version of this article.)

acquired using the Inveon Acquisition Workplace (IAW) software 2.0. Unless otherwise stated, the X-ray source was set at 30 kV and the current at 0.5 uA. Scans were done with 180 projections at full rotation using medium-high magnification and a binning factor of 2. The exposure time was 2350 ms per projection, with a total scan time of approximately 12 min. The μCT images were reconstructed with the Hamming algorithm and no denoising using IAW software, resulting in an isotropic voxel size of 44 μm. The images were calibrated in Hounsfield units (HU), where air and water were defined as −1000 and 0 HU, respectively. Isotropic total variation (ITV) denoising [14], modified such that all immediate surrounding voxels in 3D space were taken into account when determining the proximity operator, was applied to the images. The μCT data were analysed using the Inveon Research Workplace (IRW) software. Voxel data for regions of interest (ROIs) were exported and assessed using Matlab.

2.3. Portable-NMR measurements

Immediately following μCT, the breast tissue pieces were briefly blotted with lint-free tissue and placed in a dry 24-well plate and each examined in isolation using the NMR-Mouse PM25 (Magritek, Wellington, New Zealand), a single-sided NMR scanner using a permanent magnet with a horizontal magnetic field $B_0 = 0.31$ T and a vertical permanent magnetic field gradient $g = 7.5$ T/m [12,13,15,16]. A surface coil was used to excite and detect the NMR signal. The thickness of the sensing slice was ~100 μm. T_1 measurements were made using a saturation recovery pulse sequence consisting of a train of 90° pulses used to saturate the longitudinal magnetization, followed by a variable saturation-recovery period (T_{SR}), a CarrPurcell-Meiboom-Gill detection block, and a fixed recovery time TR = 2000 ms. The saturation recovery curve was sampled at 30 T_{SR} values exponentially spaced between 40 and 3000 ms. The T_1 datasets were analysed using a three-parameter monoexponential least-squares fit [12]. A Carr-Purcell-Meiboom-Gill sequence (echo time TE = 70 μs with NE = 64 echoes) was used for signal detection with the number of averages NS = 4.

T_2 measurements were made using the CPMG pulse sequence with TE = 70 μs, NE = 4096, NS = 8 and TR = 30,000 ms. The T_2 datasets were analysed using a three-parameter monoexponential least-squares fit as well as an inverse Laplace transform (ILT) [13].

Diffusion measurements were made using a stimulated-echo (STE) diffusion-encoding block (diffusion interval Δ = 10 ms, 32 equidistant values of STE echo time τ ranging from 0.05 to 1 ms) and a CPMG detection block (TE = 70 μs, NE = 64, NS = 8 and TR = 2000 ms). The relative apparent amounts of water and fat were quantified based on a biexponential ("two-pool") analysis of the diffusion attenuation curves, where the rate of the initial diffusive decay represents the weighted average of the "fast" (water) and the "slow" (fat) diffusion coefficients; the terminal decay yields the weight and the diffusion coefficient of the "slow" component; and the weight of the fast-diffusing component can be determined by subtracting the "slow" contribution from the initial weighted-average decay [17]. The weights of the fast-diffusing and slow-diffusing components thus determined were attributed to water and fat, respectively. The biexponential analysis was performed using three different numerical approaches: (1) Linear least-squares fitting of the initial and the terminal signal decay regions in Stejskal-Tanner plots [17]; (2) Nonlinear biexponential least-squares fitting of the Stejskal-Tanner plots; and (3) Nonlinear biexponential least-squares fitting of the original non-linearised plots, Signal *vs* τ. The results of the three approaches were used for cross-validation and evaluation of the true uncertainties of the relative amounts of water and fat components in the tissue samples.

The total measurement times were 5 min, 4 min and 8.5 min for each T_1, T_2 and diffusion measurement, respectively. T_1 and T_2 measurements were made at either 2 or 3 different depths in each sample, while diffusion measurements were made at either 1 or 2 depths.

2.4. Statistics

Pearson's r coefficients and the respective *p* values were calculated using GraphPad Prism 7.

3. Results

3.1. Optimisation of μCT scan protocol for breast tissue density profiling

We first established the μCT protocol for breast tissue explants that would enable optimal quantification of HMD and LMD areas. A piece of non-malignant breast tissue, confirmed to contain both HMD and LMD regions by H&E staining (Fig. 1B), was placed inside a cylindrical tube (Fig. 1A). This type of enclosed container minimises tissue dehydration during image acquisition, enables the breast explant to remain sterile, and, as the Inveon μCT scanner uses a rotating gantry, the cylindrical shape limits the generation of X-ray artefacts. Although μCT imaging of dense objects such as bone is an established technique, this is not the case with soft objects like breast explants. Therefore, we optimised the X-ray voltage by scanning the same breast explant at 30 kV, 60 kV and 80 kV, while keeping the X-ray photon counts consistent. The objective was to identify the voltage that provides the greatest image contrast between the HMD and LMD regions and most effectively enables differentiation between HMD and LMD regions in the HU histograms. We also compared two reconstruction algorithms (Shepp-Logan and Hamming, both performed using Inveon software), and determined that the Hamming algorithm gave clearer images (data not shown). Images were denoised by applying a modification of the ITV algorithm. Based on the HU histograms, which depict the number of voxels within the reconstructed 3D image that exhibit a particular HU value, the 30 kV voltage provided the greatest spread of HU values, enabling clear separation of the histogram peaks corresponding to HMD from LMD regions (Fig. 1C). An increase in the voltage led to a reduction in the HU value range as well as the degree of contrast in the μCT images (Fig. 1D). As expected, post-ITV reconstruction provided smoother images (Fig. 1D) and more defined peaks (Fig. 1C), hence all subsequent images were analysed with ITV applied.

3.2. Intra-sample comparison of NMR and μCT measurements of mammographic density

After establishing that the 30 kV protocol best differentiated HMD from LMD tissue, we scanned pieces of breast tissue obtained from prophylactic mastectomies from two women. Regions of high, medium

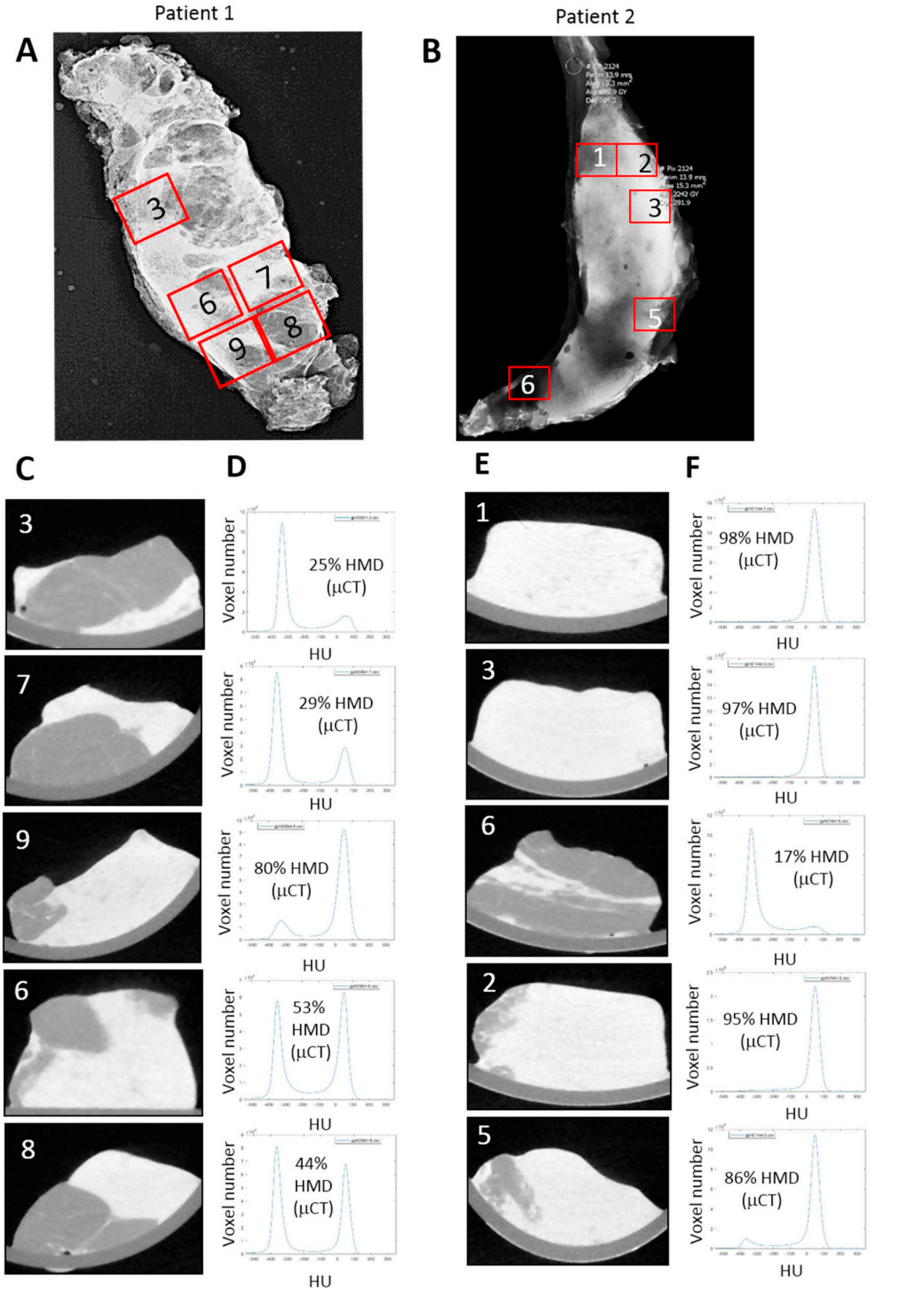

(caption on next page)

Fig. 2. MicroCT (μCT) of patient tissue of varying densities. Breast slice mammogram depicting where each of the breast pieces were taken for patient 1 (A) and patient 2 (B). C. Post-ITV de-noising was applied to images of patient 1 breast pieces (D) and patient 1 density distribution plots with the % HMD (μCT) value were overlaid. E. Post-ITV de-noising was applied to images of patient 2 breast pieces with (F) and patient 2 density distribution plots with the % HMD (μCT) value overlaid.

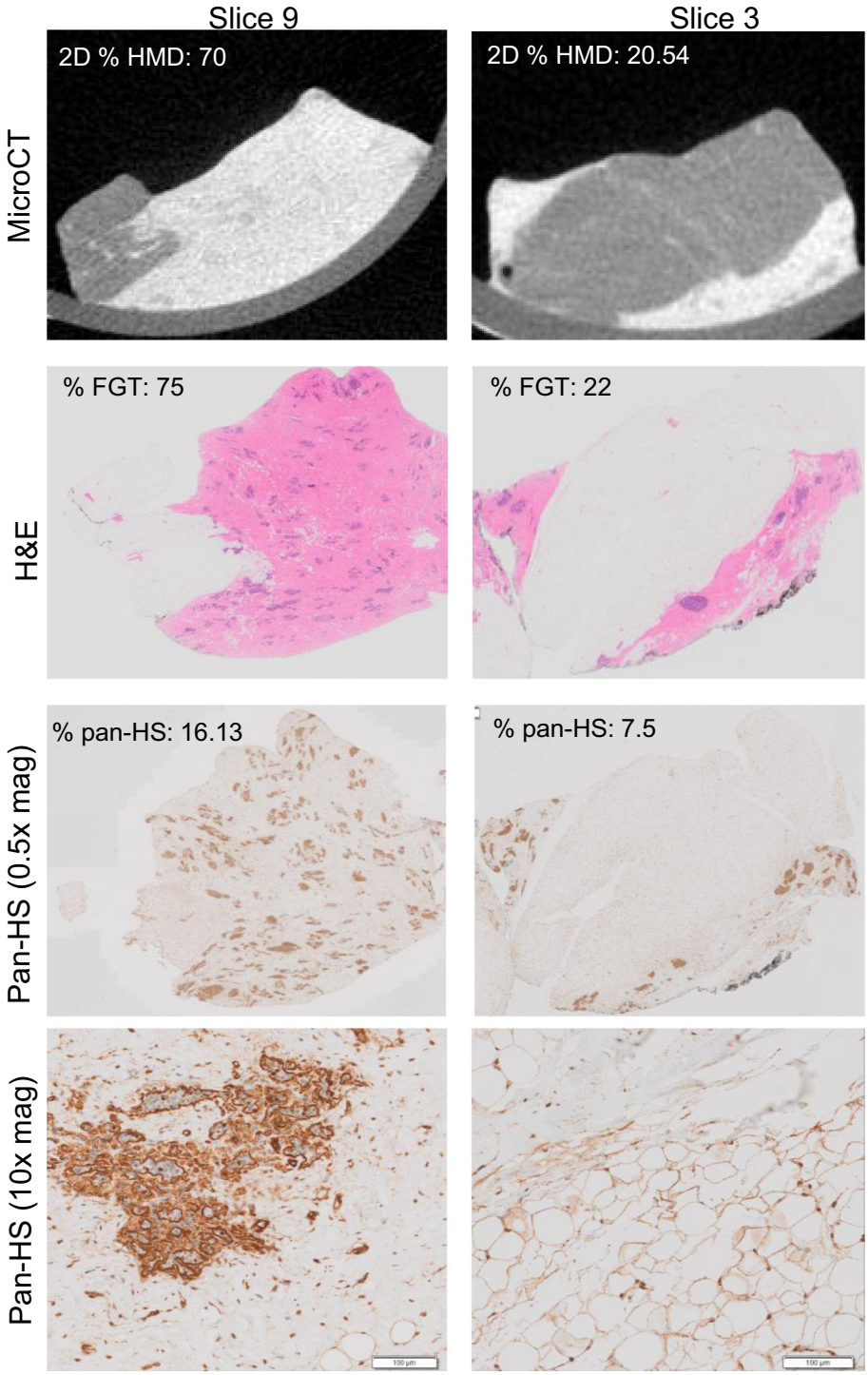

Fig. 3. Histological images of the slices from Figure 2 part C. High-MD tissue has an increased HSPG abundance and hence greater water carrying capacity. Correlation between % HMD 2D optical slice, and comparable slices stained with haematoxylin and eosin to quantify fibroglandular tissue (stroma and glands) and Pan-HS antibody which detects all HSPG proteins.

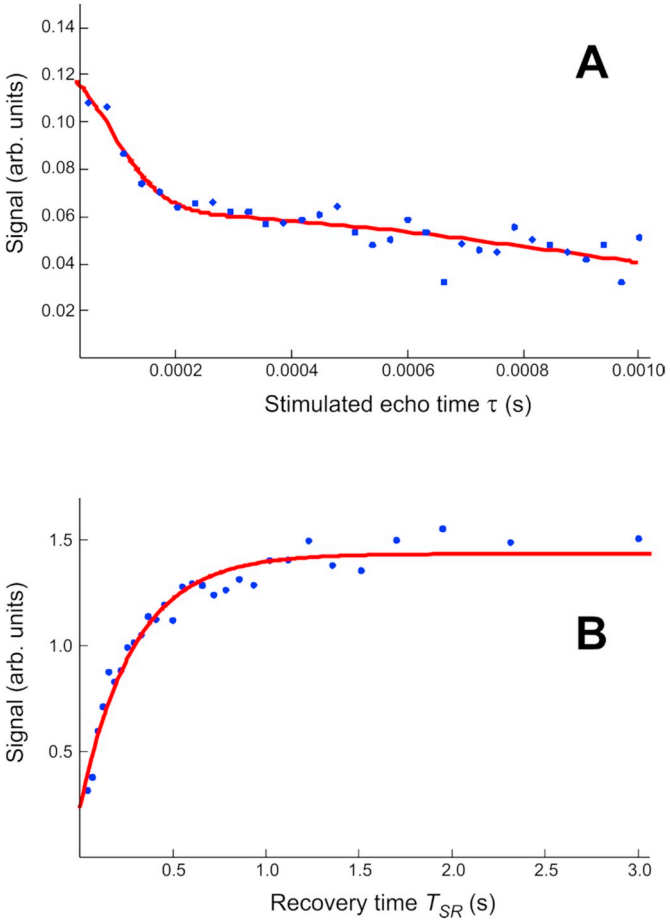

Fig. 4. Nonlinear least-squares fits of representative (A) diffusion and (B) T_1 datasets (both datasets were acquired from the same slice within the same sample). The fit of the diffusion dataset was performed using the two-pool ("biexponential") model, where the Fat component was assumed to exhibit a single diffusion coefficient, while the Water component was assumed to exhibit a different but also a single diffusion coefficient. The fit of the T_1 dataset was performed using a monoexponential model, where the effective 1/T1 was treated as the weighted-average of the 1/T1 values of Fat and Water. All diffusion and T_1 datasets in the present study were fitted using these respective models. The Figure demonstrates the absence of significant systematic deviations in both types of fits, and thus demonstrates the suitability of each fitting model for the respective type of data.

and low MD were excised from a breast tissue slice as described in Section 2.1. The samples were taken from various regions of the breast slices obtained from two different patients who had similar demographic information. The locations of the excised samples are shown in Fig. 2A and B, while the corresponding post-reconstruction ITV μCT images and HU distribution plots are shown in Fig. 2C–F.

Consistent with Fig. 1, HU histogram plots of both HMD and LMD tissue regions were bimodal, with two distinct and well-resolved peaks in the HU distribution plots with the maxima near +60 HU and −320 HU, respectively. Cross-sectional μCT images of tissue that appeared predominantly bright (*e.g.* Fig. 2E panel 1) had a high % HMD in the HU histograms. In contrast, images which appeared predominantly to have mid-range intensities (*e.g.* Fig. 2E panel 6) had a low % HMD. Regions with an even mix of bright and mid-range intensities had approximately 50% HMD in the HU histograms (*e.g.* Fig. 2C panel 6).

Detailed histological examination of slices 9 and 3 from part C in Fig. 2 revealed key correlative information (Fig. 3): Fibroglandular content (non-fat tissue) correlated well with *2D microCT* derived from the depicted slice. In addition, and the slice with greater %HMD had a greater abundance HSPG proteins of all type (pan-HS), proteins which are known to sequester several water molecules per unit of protein.

The entire sample set shown in Fig. 2 were then analysed using the NMR-Mouse in order to measure the T_1 and T_2 values and diffusion attenuation curves of the samples. The relative fat and water amounts were measured from the diffusion attenuation curves as described in Methods section. The T_1 recovery curves and the T_2 decay curves exhibited monoexponential behaviour. Fig. 4 shows the least-squares fits of representative diffusion and T_1 datasets: Fig. 4A demonstrates the suitability of the two-pool ("biexponential") model for the diffusion data, while Fig. 4B demonstrates the suitability of the monoexponential model for the T_1 data. The T_2 spectra obtained from ILT failed to separate fat and water peaks; the ILT results were therefore not used in the subsequent analysis.

The results are summarised in Fig. 5. Fig. 5A depicts where the three NMR measurements were taken through the tissue sample. Fig. 5B shows the correlation between the T_1 values and the relative amount of high-MD tissue (% HMD) determined from the μCT HU distributions. Fig. 5C shows the correlation between the T_2 values of the same samples and the % HMD values measured using μCT. Fig. 5D shows the correlation between the T_1 values and the relative water content obtained from NMR diffusion analysis. Fig. 5E shows the correlation between the T_2 values and the relative water content measured from diffusion NMR. Fig. 5F shows the correlation between the relative water content obtained from NMR diffusion analysis and the % HMD determined from the μCT HU distribution plots. All the correlations were statistically significant ($p < 0.05$). However, the three pairwise correlations involving T_1 values, NMR diffusion-derived water content and μCT-derived tissue composition were significantly stronger than either of the correlations involving T_2. The correlation between NMR-diffusion water content and μCT %HMD exhibited the highest concordance, with $R^2 = 0.96$ (Fig. 5F). T_1 values exhibited a good correlation with both NMR-diffusion water content ($R^2 = 0.94$, Fig. 5D) and μCT % HMD ($R^2 = 0.92$, Fig. 5B). T_2 values exhibited a modest correlation with both those benchmarks ($R^2 = 0.63$, Fig. 5E, and $R^2 = 0.61$, Fig. 5C, respectively).

4. Discussion

In our previous work we demonstrated that portable NMR-measured T_1 values of excised breast tissue samples enable reliable discrimination between HMD and LMD tissue regions [12]. Subsequently we have shown that the relative areas of the fat and water peaks in inverse Laplace transform (ILT) T_2 spectra similarly enabled reliable discrimination between HMD and LMD regions [12,13]. In the current study we investigated whether quantitative portable NMR could be used to quantify breast tissue density on a *continuous* scale (0% to 100%) as opposed to the binary HMD/LMD classifications employed in our previous studies. The relative areas of HMD and LMD peaks in the HU distributions derived from volumetric μCT measurements were used as the "gold standard" in the present study. Based on this gold standard, we found that both T_1 and diffusion portable-NMR measurements could be successfully used for continuous-valued quantification of MD in the excised samples. Across a set of excised breast tissue samples with a broad range of mammographic densities, the T_1 values correlated strongly with the % HMD measured from μCT ($R^2 = 0.92$, $p < 0.0001$), while the relative water content measured from diffusion NMR exhibited an even stronger correlation with the μCT data ($R^2 = 0.96$, $p < 0.0001$). The T_1 and diffusion NMR results were also strongly correlated with each other ($R^2 = 0.94$, $p < 0.0001$).

We found that the samples' mean T_2 values exhibited only a modest correlation with both the μCT results ($R^2 = 0.61$, $p < 0.0127$) and with diffusion NMR results ($R^2 = 0.63$, $p < 0.0109$). This can be attributed to the fact that, unlike our previous T_2 study [13], the T_2 measurement

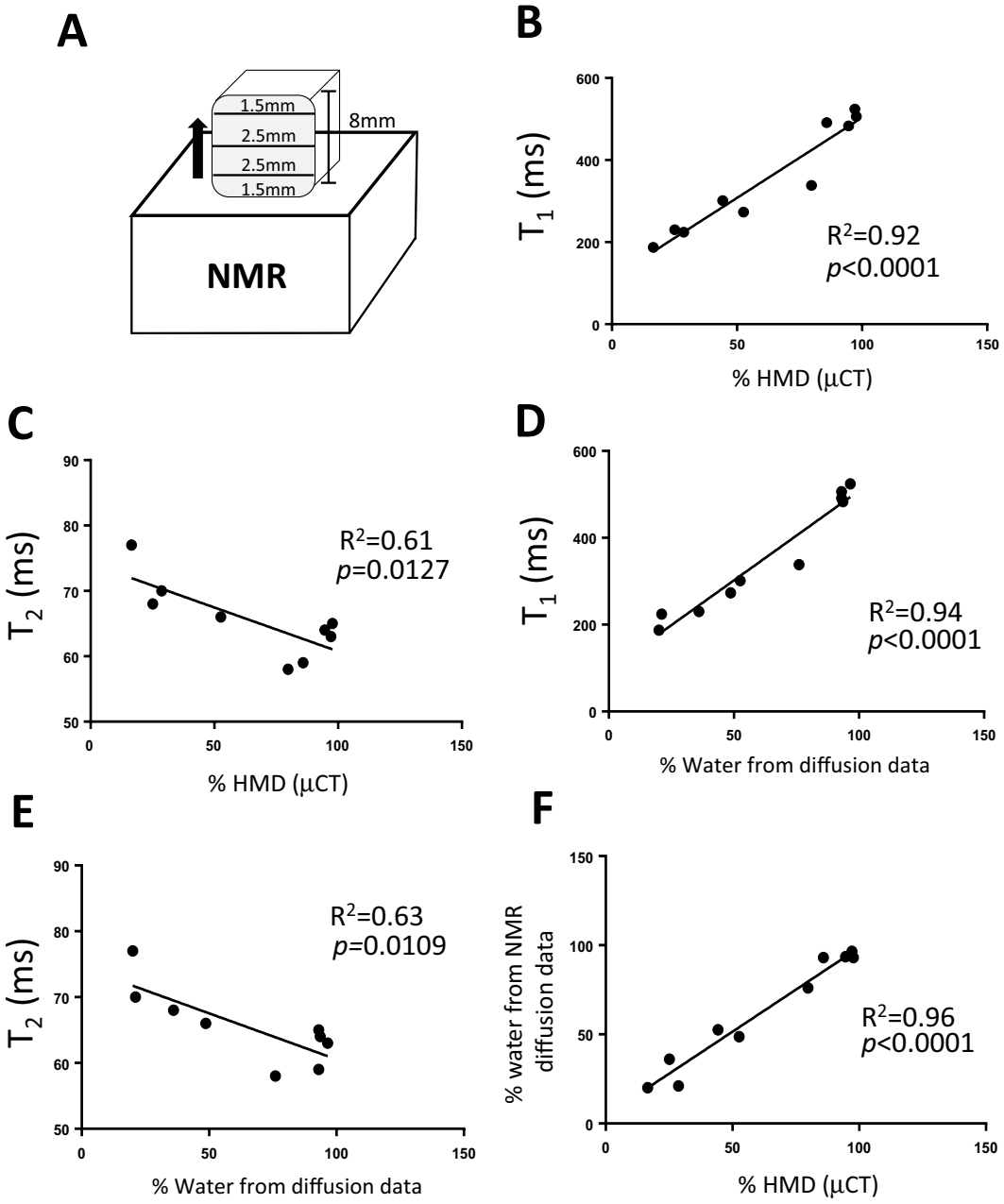

Fig. 5. NMR T_1 *vs* % HMD (μCT) of patient tissue slices. Location and spacing from which each of the NMR measurements was taken, A. % HMD (mCT) correlated more strongly with T_1, B, rather than T_2 values, C. % water from NMR diffusion data also correlated with T_1, D, rather than T_2 values, E, in the tissue samples. F. % HMD (mCT) showed the strongest correlation of all with % water determined from NMR diffusion data. Shown is the Pearson's coefficient squared (R^2) and its associated *p* value. All portable-NMR quantities are reported as the values averaged over the number of slices used.

conditions employed in the present study did not enable separation between the fat and water peaks in T_2 relaxation spectra. This, in turn, can be attributed to a combination of the relatively short CPMG echo times used in the present study (60 μs *vs* 120 μs previously) and the relatively low magnetic field gradient of the PM25 NMR-Mouse model (7.5 T/m *vs* 22.5 T/m for the PM5 model used previously). The inverse T_2 values of water measured in portable NMR are dominated by the diffusion contribution [18]:

$$\frac{1}{T_2} = \frac{1}{T_{2True}} + \frac{D\,\gamma^2 g^2}{12} TE^2 \quad (1)$$

Therefore, the combination of lower *g* and shorter *TE* selected would have resulted in a lengthening of the water T_2 values, resulting in an overlap of the fat and water peaks in the T_2 spectra. We emphasise that this does not disqualify T_2 as a MD metric: the ability of the T_2 spectra to differentiate between HMD and LMD regions has been demonstrated in our previous study [13]. Rather, this negative result demonstrates the importance of careful selection of portable-NMR measurement parameters for MD quantification. We postulate that CPMG T_2 data acquired on a PM25 NMR-Mouse model with a longer TE (~500 μs) would be suitable for MD quantification.

We note that the correlation between portable-NMR and μCT data is good despite the fact that the μCT data were volumetric (acquired from the entire volume of the sample) but the portable-NMR data were acquired from a small number of thin (~100 um) slices. Therefore, even in the presence of a perfect intrinsic agreement between the two methods, the differences in the volumes sampled could potentially

result in differences in the apparent MD-equivalent quantities obtained from the two techniques. However, examination of Fig. 5 suggests that even if such differences were present, they were very small, and there was little “sampling bias” in the portable-NMR results. This can be attributed to the fact that MD spatial patterns within breast tissue are usually irregular, and therefore portable-NMR signal can be expected to undergo effective averaging over HMD and LMD domains present within the tissue. This suggests that, under normal conditions, the apparent MD values obtained from portable NMR can be expected to have little sensitivity to the exact selection of the sampling slice(s).

Overall, these results may indicate the potential utility of portable NMR in measuring and monitoring MD, however considerable further testing is needed to validate this claim. This includes, first and foremost, clinical *in vivo* testing.

Further benefits of the present study include the optimisation of an approach to obtain equivalent 3D measures using μCT instead of mammography to determine MD, which has a number of advantages in the research setting. In doing so, we have established a reliable protocol in which we now are able to (1) present X-ray images in which machine noise is minimized using a combination of reconstructing *via* the Hamming algorithm and post-reconstruction denoising *via* a modified ITV algorithm, (2) present a graph of density distribution within the sample and (3) accurately provide volumetric % HMD values of the tissue. This refined measurement and analysis methodology opens up the possibility of using μCT on cultured breast tissue explants [19,20] to quantify changes in either % HMD, or changes in the total volumetric size of the LMD and HMD regions within tissue explants over experimental time courses.

The results of this study support our previous finding that high-MD tissue has a higher volume fraction of tissue water than low-MD tissue (see Fig. 5). This is most likely due to water being the predominant chemical component (both intra- and extracellular) of FGT. Our current finding that % HMD is positively and apparently linearly correlated with the tissue water content is consistent with the ability of long proteoglycan chains to osmotically attract and sequester water molecules [21]. Consistent with this, we found that heparin sulphate proteoglycans were in greater abundance in higher %HMD than in lower % HMD samples (Fig. 3). Further to this, Stoeckelhuber and colleagues reported that breast tissue swells during the luteal phase of the menstrual cycle, the phase associated with a slight increase in breast density [22]. Proteoglycans also sequester growth factors, which can be released by actively growing breast tumours *via* their expression of heparanase. This provides a potential molecular mechanism for proteoglycans' (and therefore HMD tissue's) ability to contribute to the breast cancer risk [23].

Our data suggest that it may be possible for this the portable-NMR approach to be used to investigate MD *change* in response to biochemical, enzymatic or hormonal treatments. Such work could be performed on human breast tissue cultured *ex vivo*, as has been done to investigate human breast cancer responses to hormonal stimulation [19,20]. NMR measurements do not physically alter the tissue; these measurements could therefore be performed both at the baseline, intermediate time points and at the endpoint, allowing longitudinal analysis of the same tissue sample.

Furthermore, the results of the current study support the use of portable NMR as a means of monitoring MD in human subjects, which could either complement or serve as an alternative to standard mammography. Studies comparing mammography, non-contrast MRI and NMR-Mouse measurements of the upper-outer quadrant region of the breast in healthy female subjects are underway, in order to test the sensitivity of the NMR-Mouse in predicting MD. Clinical utility of this novel technology could lie in early assessment of MD status for assisting in breast cancer risk prediction [24], and in monitoring MD change in women undergoing anti-oestrogen therapies for prevention of adjuvant therapy of breast cancer [8]. In these clinical scenarios subtle early changes in MD may be an early indication of the efficacy of the treatment [8]. The use of portable NMR for MD quantification in the course of these therapies could enable non-responding patients to be identified early in the 5 or 10 year treatment regimen.

5. Conclusion

The results of the current study demonstrate the utility of portable-NMR T_1 and diffusion measurements for quantification of MD in excised breast tissue samples. Both T_1 values and the relative water content derived from diffusion measurements exhibited excellent quantitative correlation with the relative HMD tissue content derived from volumetric μCT measurements over the full range of MD values. The results provide further support for the use of portable NMR for MD screening and monitoring.

Acknowledgements

The authors wish to acknowledge Ms. Gillian Jagger, clinical research nurse, Department of Radiology, Princess Alexandra Hospital, for co-ordinating the accrual of patients into this study. Thanks also go to the women who donated their breast tissue to facilitate this study. The authors wish to thank Professor Graham Galloway, Director of Imaging Technology at the Translational Research Institute, for his guidance in the early stages of this study. This work is funded by the Princess Alexandra Hospital Research Foundation Translational Research Innovation Award. The authors also acknowledge the Translational Research Institute (TRI) for providing the excellent research environment and core facilities that enabled this research. The Translational Research Institute receives support from the Australian Federal Government.

References

[1] World Health Organisationeditor. WHO position paper on mammography screening. Switzerland: WHO Press; 2014. p. 1–78. World Health Organisation, Editor.
[2] Breast Screen Australia. Position statement on breast density and screening within the breast screen Australia program. Australian Government Department of Health; 2016. Editor.
[3] Sickles, E.A., C.J. D'Orsi, and B. L.W., Mammography, in ACR BI-RADS® Atlas, Breast imaging reporting and data system. 2013, American College of Radiology: Reston, VA. p. 20.
[4] Carney PA, et al. Individual and combined effects of age, breast density, and hormone replacement therapy use on the accuracy of screening mammography. Ann Intern Med 2003;138(3):168–75.
[5] Hopper JL. Odds per adjusted standard deviation: comparing strengths of associations for risk factors measured on different scales and across diseases and populations. Am J Epidemiol 2015;182(10):863–7.
[6] Sprague BL, et al. Prevalence of mammographically dense breasts in the United States. J Natl Cancer Inst 2014;106(10):1–6.
[7] Boyd NF, et al. Mammographic density and the risk and detection of breast cancer. N Engl J Med 2007;356(3):227–36.
[8] Shawky MS, et al. Mammographic density: a potential monitoring biomarker for adjuvant and preventative breast cancer endocrine therapies. Oncotarget 2017;8(3):5578–91.
[9] Mullooly M, et al. Mammographic density as a biosensor of tamoxifen effectiveness in adjuvant endocrine treatment of breast cancer: opportunities and implications. J Clin Oncol 2016;34(18):2093–7.
[10] Elsamany S, et al. Mammographic breast density: predictive value for pathological response to neoadjuvant chemotherapy in breast cancer patients. Breast 2015;24(5):576–81.
[11] Hugo HJ, et al. Looking beyond the mammogram to assess mammographic density: a narrative review. Biomed Spectrosc Imaging 2018;7(1–2):63–80.
[12] Tourell MC, et al. T1 -based sensing of mammographic density using single-sided portable NMR. Magn Reson Med 2018;80(3):1243–51.
[13] Ali TS, et al. Transverse relaxation-based assessment of mammographic density and breast tissue composition by single-sided portable NMR. Magn Reson Med 2019;82(3):1199–213.
[14] Micchelli CA, Lixin S, Xu Y. Proximity algorithms for image models: denoising. Inverse Probl 2011;27(045009):1–30.
[15] Blumich B, et al. The NMR-mouse: construction, excitation, and applications. Magn Reson Imaging 1998;16(5–6):479–84.

[16] Blumich B, Perlo J, Casanova F. Mobile single-sided NMR. Prog Nucl Magn Reson Spectrosc 2008;52(4):197–269.
[17] Momot KI, Kuchel PW. Pulsed field gradient nuclear magnetic resonance as a tool for studying drug delivery systems. Concepts Magn Reson Part A 2003;19a (2):51–64.
[18] Van Landeghem M, et al. Low-gradient single-sided NMR sensor for one-shot profiling of human skin. J Magn Reson 2012;215:74–84.
[19] Dean JL, et al. Therapeutic response to CDK4/6 inhibition in breast cancer defined by ex vivo analyses of human tumors. Cell Cycle 2012;11(14):2756–61.
[20] Mohammed H, et al. Progesterone receptor modulates ERalpha action in breast cancer. Nature 2015;523(7560):313–7.
[21] Iozzo RV, Schaefer L. Proteoglycan form and function: a comprehensive nomenclature of proteoglycans. Matrix Biol 2015;42:11–55.
[22] Stoeckelhuber M, et al. Proteoglycan-collagen associations in the non-lactating human breast connective tissue during the menstrual cycle. Histochem Cell Biol 2002;118(3):221–30.
[23] Shawky MS, et al. Proteoglycans: potential agents in mammographic density and the associated breast cancer risk. J Mammary Gland Biol Neoplasia 2015;20(3–4):121–31.
[24] van Veen EM, et al. Use of single-nucleotide polymorphisms and mammographic density plus classic risk factors for breast cancer risk prediction. JAMA Oncol 2018;4(4):476–82.